Phenol-pyrazole ligands in the design of manganese(III) compounds : synthesis, structural characterization and study of the magnetic properties

Viciano Chumillas, Marta

Chapter 4

From 1-D to isolated trinuclear compounds: impact of the co-ligand and the carboxylate on the core $[Mn_3(\mu_3\text{-}O)(phpzR)_3]^{+}$*

The effects of the co-ligand and the carboxylate on the trinuclear core $[Mn_3(\mu_3\text{-}O)(phpzR)_3]^{+}$ have been studied with the synthesis of three new compounds, $[Mn_3(\mu_3\text{-}O)(phpzMe)_3(O_2CMe)(EtOH)]\cdot EtOH$ (**13**), $^{n}Bu_4N[Mn_3(\mu_3\text{-}O)(phpzMe)_3(O_2CPh)_2]$ (**14**) and $^{n}Bu_4N[Mn_3(\mu_3\text{-}O)(phpzPh)_3(O_2CPh)_2]$ (**15**). Hydrogen bonding interactions between the trinuclear units of **13** result in a 1-D chain structure. Compounds **14** and **15** are isolated trinuclear units. Magnetic susceptibility studies indicate the presence of both antiferromagnetic and ferromagnetic interactions in compound **13**, while only antiferromagnetic interactions are found in compounds **14** and **15**. The ferromagnetic interactions in the trinuclear unit have been ascribed mainly to the distortion of the Mn–O–Mn angle of the core $[Mn_3(\mu_3\text{-}O)(phpzR)_3]^{+}$.

* Part of this chapter has been published in the literature: Viciano-Chumillas M., Tanase S., Mutikainen I., Turpeinen U., de Jongh L.J., Reedijk J., *Dalton Trans.,* **2009***,* 7445-7453.

4.1. Introduction

Oxide-centred trinuclear manganese(III) compounds are well known for several years in the literature.[1] The first reported compounds were commonly named basic carboxylates and they have the general formula $[Mn_3(\mu_3\text{-}O)(O_2CR)_6L_3]^+$ (R = Me, Et, Pr, Piv, Ph, and L = py, 3-Mepy, Im, H_2O).[1-6] Lately, the carboxylate ligands and solvent molecules have been replaced by other types of ligands, such as salicylaldoxime,[7-11] or pyrazole derivatives,[12-16] thereby extending the group of trinuclear manganese(III) compounds. All these compounds show predominant antiferromagnetic interactions between the manganese(III) ions, with the exception of those containing oximato-based ligands[7,8,11,17-19] and the compound $[NEt_3(CH_2Cl)]_2[Mn_3(\mu_3\text{-}O)(Hhmc)_3(H_2hmc)_3]$ (H_3hmc = 2,6-bis(hydroxymethyl)-*p*-cresol)[20], in which ferromagnetic interactions are operative. Due to the complexity of the magnetic exchange paths, several factors have been proposed as the origins of the observed ferromagnetic behaviour.[16,17,20,21] An important cause appears to be the distortion of the $[Mn_3(\mu_3\text{-}O)]^{7+}$ core, where the Mn–O–Mn angle is smaller than 120º (value for an equilateral triangle);[16,17,21] a switch from antiferromagnetic to ferromagnetic exchange is observed at angles below approximately 120º.[22] The displacement of the $\mu_3\text{-}O^{2-}$ ion from the plane formed by all manganese(III) ions seems also to be an important factor for the presence of ferromagnetic interactions.[20] It has been shown that the ligand distortion, *i.e.* the Mn–N–O–Mn torsion angle in oximate ligands, plays an important role as well; a larger torsion angle giving rise to a stronger ferromagnetic coupling.[7,8,17,21]

In Chapter 3,[16] some trinuclear manganese(III) compounds obtained with mononuclear manganese(III) building blocks containing phenol-pyrazole ligands were described. Temperature-dependent magnetic susceptibility studies have revealed that the antiferromagnetic intramolecular interactions are dominant in most of the cases, with the exception of one compound that displays both antiferromagnetic and ferromagnetic interactions between the manganese(III) ions.[16] In the later case, the ferromagnetic exchange interaction was found to correspond to the major distortion of the Mn–O–Mn angle of the $[Mn_3(\mu_3\text{-}O)]^{7+}$ core. In the present chapter, a new approach is reported within the strategy of modifying known complexes, *i.e.* the controlled distortion of the $[Mn_3(\mu_3\text{-}O)]^{7+}$ core to elucidate the crucial magnetic exchange paths. In this respect, the effect of different carboxylate ligands and co-ligands on the geometry of the $[Mn_3(\mu_3\text{-}O)]^{7+}$ core has been studied. Three new trinuclear manganese(III) compounds, $[Mn_3(\mu_3\text{-}O)(phpzMe)_3(O_2CMe)(EtOH)]\cdot EtOH$ (**13**), $^nBu_4N[Mn_3(\mu_3\text{-}O)(phpzMe)_3(O_2CPh)_2]$ (**14**) and $^nBu_4N[Mn_3(\mu_3\text{-}O)(phpzPh)_3(O_2CPh)_2]$ (**15**) are presented and their synthesis, X-ray crystal structures and magnetic properties are described in detail.

4.2. Experimental Section

General remarks. Starting materials were purchased from Aldrich. All manipulations were performed using materials as received. $Mn(O_2CPh)_2{\cdot}2H_2O$,[23] $^nBu_4NMnO_4$[5] and the ligands 3(5)-(2-hydroxyphenyl)-5(3)-methylpyrazole (H_2phpzMe) and 3(5)-(2-hydroxyphenyl)-5(3)-phenylpyrazole (H_2phpzPh) have been synthesized according to reported procedures.[24]

General synthetic procedure

Solid $^nBu_4NMnO_4$ (0.07 mmol) was added to a solution of $Mn(O_2CR')_2{\cdot}nH_2O$ (R' = Me, Ph) (0.28 mmol) in ethanol. The resulting solution was stirred for a few minutes, followed by the addition of H_2phpzR (R = Me, Ph) (0.21 mmol) in ethanol. The solution mixture resulted in the formation of a brown precipitate, which was filtered off and discarded. The filtrate was allowed to evaporate slowly, affording brown crystals within a few days in all cases. The crystals were collected by filtration, washed with Et_2O and dried in vacuum.

$[Mn_3(\mu_3\text{-}O)(phpzMe)_3(O_2CMe)(EtOH)]{\cdot}EtOH$ (13). Yield: 17% (30 mg). Anal. Calcd for **13** ($C_{36}H_{39}Mn_3N_6O_8$): C, 50.96; H, 4.63; N, 9.90. Found: C, 50.53; H, 5.05; N, 9.90. IR (ν_{max}/cm^{-1}): 3070(w), 1597(m), 1560(m), 1550(m), 1530(s), 1496(m), 1458(s), 1322(m), 1296(vs), 1268(vs), 1249(vs), 1144(w), 1127(s), 1090(m), 1062(m), 1036(s), 982(w), 864(s), 792(s), 784(m), 752(s), 742(s), 725(s), 668(vs), 647(vs), 601(vs), 484(m), 418(s), 381(s), 312(s).

$^nBu_4N[Mn_3(\mu_3\text{-}O)(phpzMe)_3(O_2CPh)_2]$ (14). Yield: 11% (28 mg). Anal. Calcd for **14** ($C_{60}H_{70}Mn_3N_7O_8$): C, 60.97; H, 5.97; N, 8.29. Found: C, 60.47; H, 6.78; N, 8.36. IR (ν_{max}/cm^{-1}): 2964(m), 2875(w), 1594(s), 1563(s), 1558(vs), 1540(m), 1531(m), 1494(s), 1456(vs), 1374(vs), 1330(m), 1296(vs), 1268(vs), 1254(vs), 1152(m), 1127(s), 1088(m), 1064(s), 1056(s), 1034(s), 988(m), 938(m), 866(s), 834(m), 782(m), 766(s), 760(s), 752(vs), 720(vs), 680(vs), 668(vs), 642(vs), 612(s), 580(s), 542(m), 442(s), 422(s), 417(s), 379(vs), 350(s), 334(s).

$^nBu_4N[Mn_3(\mu_3\text{-}O)(phpzPh)_3(O_2CPh)_2]$ (15). Yield: 13% (37 mg). Anal. Calcd for **15** ($C_{75}H_{76}Mn_3N_7O_8$): C, 65.84; H, 5.60; N, 7.17. Found: C, 65.21; H, 6.37; N, 7.21. IR (ν_{max}/cm^{-1}): 2962(m), 2880(w), 1595(s), 1564(m), 1558(vs), 1539(m), 1532(m), 1506(m), 1476(vs), 1456(s), 1448(s), 1428(m), 1378(vs), 1297(s), 1266(s), 1249(s), 1175(w), 1122(s), 1098(s), 1026(m), 995(m), 935(w), 864(s), 836(w), 797(m), 752(s), 719(vs), 710(s), 696(vs), 686(s), 668(vs), 662(s), 646(s), 610(m), 588(m), 534(m), 492(w), 456(m), 448(m), 435(m), 421(s), 378(m), 374(m), 333(s).

Physical Measurements. Elemental analyses for C, H and N were performed on a Perkin-Elmer 2400 series II analyzer. Infrared spectra (4000–300 cm^{-1}) were recorded on a Perkin-Elmer Paragon 1000 FTIR spectrometer equipped with a Golden Gate ATR device, using the reflectance technique. DC and AC magnetic data were recorded using a Quantum Design MPMS-5 SQUID susceptometer. The magnetic susceptibilities were measured from 1.8 to 300 K on powdered single-crystal samples in a gelatine capsule with an applied field of 0.1 T. The magnetization was measured from 2 up to 20 K in the 0–5 T range. Data were corrected for magnetization of the sample holder and for diamagnetic contributions, which were estimated from Pascal's constants.[25]

X-ray Crystallography. Intensity data for single crystals of **13**, **14** and **15** were collected using MoKα radiation (λ = 0.71073 Å) on a Nonius KappaCCD diffractometer. Crystal and refinement data for **13, 14** and **15** are collected in Table 4.1. The intensity data were corrected for Lorentz and polarization effects, and for absorption (multiscan absorption correction[26]). The structures were solved by Patterson methods.[27] The programs EvalCCD,[28,29] DIRDIF96,[30] SHELXS-97[31] and SHELXL-97[32] were used for data reduction, structure solution and refinement, respectively. All non-hydrogen atoms were refined with anisotropic displacement parameters. Geometric calculations and molecular graphics were performed with the PLATON package.[33]

4.3. Results and Discussion

Synthesis. μ_3-oxide bridged trinuclear manganese(III) compounds have been previously obtained by reacting mononuclear manganese(III) building blocks, containing phenol-pyrazole ligands, with manganese(II) acetate or with sodium azide (see Chapter 3).[16] These compounds contain the same core with the general formula $[Mn_3(\mu_3\text{-}O)(phpzR)_3]^+$; methanol molecules, and acetate or azide bridging ligands have been found at the terminal positions. In the present chapter, the influence of a different carboxylate ligand, namely benzoate and a different starting solvent, namely ethanol, in these type of trinuclear manganese(III) compounds is presented. In addition, new synthetic routes have been explored by starting from manganese(II) carboxylate salts, $^nBu_4NMnO_4$ and phenol-pyrazole ligands in the same reaction. Manganese(II) salts together with $^nBu_4NMnO_4$ are an excellent and well known starting source to generate manganese(III) and/or manganese(IV) ions; depending on the used ratio, complexes of different nuclearities can be obtained.[5,23] The manganese(II)/manganese(VII) ratio employed can be either 4/1 or 3/1. The presence of $^nBu_4N^+$ in the final product is necessary to balance the charges in the compounds

$^{n}Bu_4N[Mn_3(\mu_3\text{-}O)(phpzMe)_3(O_2CPh)_2]$ (**14**) and $^{n}Bu_4N[Mn_3(\mu_3\text{-}O)(phpzPh)_3(O_2CPh)_2]$ (**15**), because there are two benzoate groups present. The use of the other $^{n}Bu_4N^+$ salts, *i.e.* $^{n}Bu_4NBr$ instead of $^{n}Bu_4NMnO_4$, did result in a decrease of the reaction yields. Compound $[Mn_3(\mu_3\text{-}O)(phpzMe)_3(O_2CMe)(EtOH)]\cdot EtOH$ (**13**) contains one acetate group only, therefore the $^{n}Bu_4N^+$ is absent. The infrared spectra of complexes **13**–**15** are very similar. The main difference is that compounds **14** and **15** exhibit the bands expected for the $^{n}Bu_4N^+$ at 2964, 2875 and 1374 cm^{-1} that are absent in compound **13**, in agreement with the X-ray crystallographic studies.

Table 4.1. Crystal data and structure refinements for $[Mn_3(\mu_3\text{-}O)(phpzMe)_3(O_2CMe)(EtOH)]\cdot EtOH$ (**13**), $^{n}Bu_4N[Mn_3(\mu_3\text{-}O)(phpzMe)_3(O_2CPh)_2]$ (**14**), $^{n}Bu_4N[Mn_3(\mu_3\text{-}O)(phpzPh)_3(O_2CPh)_2]$ (**15**).

	13	**14**	**15**
Formula	$C_{34}H_{33}Mn_3N_6O_7$, C_2H_6O	$C_{44}H_{34}Mn_3N_6O_8$, $C_{16}H_{36}N$	$C_{59}H_{40}Mn_3N_6O_8$, $C_{16}H_{36}N$
FW [g mol^{-1}]	848.55	1182.05	1368.24
Crystal system	Triclinic	Monoclinic	Triclinic
Space group	P–1	$P2_1/c$	P–1
a [Å]	8.4040(13)	12.4030(10)	13.805(2)
b [Å]	11.5702(15)	21.1640(10)	16.257(2)
c [Å]	18.427(2)	24.603(2)	16.495(2)
α [º]	98.205(10)	90	101.53(2)
β [º]	91.345(7)	120.27(1)	100.39(2)
γ [º]	93.355(11)	90	109.06(2)
V [$Å^3$]	1769.5(4)	5577.7 (9)	3305.6(10)
Z	2	4	2
D_{calc} [g cm^{-3}]	1.593	1.408	1.374
Crystal size	0.15×0.20×0.20	0.10×0.20×0.20	0.12×0.25×0.28
Number of collected reflections (unique)	28899(7338)	52922(12736)	58112(12942)
Number of observed reflections [$I_o > 2\sigma(I_o)$]	6261	8686	10168
Internal R factor	0.0280	0.048	0.055
Number of parameters	488	710	889
Goodness-of-fit S on F^2	1.05	1.05	1.08
μ [mm^{-1}]	1.118	0.731	0.627
R_1[a] [$I > 2.0\sigma(I)$]	0.0280	0.0383	0.0408
wR_2[b] [all data]	0.0696	0.0887	0.0979
T [ºC]	173	173	173

[a] $R_1 = \sum||F_o| - |F_c|| / \sum|F_o|$. [b] $wR_2 = \{\sum[w(F_o^2 - F_c^2)^2]/\sum w(F_o^2)^2\}^{1/2}$.

Description of the Molecular Structures. Compound **13** crystallizes in the triclinic space group P−1. As shown in Figure 4.1, the crystal structure reveals a trinuclear manganese(III) compound in which the three manganese(III) ions are bridged by a central oxide. Selected bond lengths and angles are listed in Table 4.2. Intracluster Mn···Mn distances are 3.153 Å, 3.330 Å and 3.300 Å for Mn(1)···Mn(2), Mn(1)···Mn(3) and Mn(2)···Mn(3), respectively. The μ_3-O^{2-} (O1) is located 0.064 Å above the Mn_3 plane. The Mn–O(1)–Mn angles are 112.65(6)º, 124.28(6)º and 122.73(7)º for Mn(1)–O(1)–Mn(2), Mn(1)–O(1)–Mn(3) and Mn(2)–O(1)–Mn(3), respectively. All the manganese(III) ions are pentacoordinated square-pyramidal based. An acetate molecule is bridging the Mn(1) and the Mn(2) ions, whereas Mn(3) contains an ethanol molecule at the axial position. In the lattice, another ethanol molecule is present, forming intermolecular hydrogen bonds with the coordinated ethanol of one trinuclear unit and also with the acetate group of a neighbouring trinuclear unit (O(5)–H(5)···O(7) = 2.591(2) Å and O(7)–H(7)···O(3) = 2.783(2) Å), thus forming a chain structure along the *a* direction (Figure 4.1). The shortest distance between the manganese(III) ions from the trinuclear units bridged by hydrogen bonding is Mn(1)···Mn(3), equal to 7.404 Å. The shortest interchain Mn···Mn distance is 6.386 Å, along the *c* direction and it belongs to a Mn(2)···Mn(2) distance.

Table 4.2. Selected bonds lengths [Å] and angles [º] for compound **13**.

Bond Lengths					
Mn(1)–O(1)	1.8979(13)	Mn(1)–O(3)	2.1026(13)	Mn(1)–O(112)	1.8377(14)
Mn(1)–N(11)	1.9375(15)	Mn(1)–N(32)	2.0175(15)	Mn(2)–O(1)	1.8911(12)
Mn(2)–O(2)	2.0794(13)	Mn(2)–O(212)	1.8257(14)	Mn(2)–N(12)	2.0195(16)
Mn(2)–N(21)	1.9518(15)	Mn(3)–O(1)	1.8689(12)	Mn(3)–O(5)	2.1458(15)
Mn(3)–O(312)	1.8247(14)	Mn(3)–N(22)	2.0385(16)	Mn(3)–N(31)	1.9679(16)
Mn(1)···Mn(2)	3.153	Mn(1)···Mn(3)	3.330	Mn(2)···Mn(3)	3.300
Bond Angles					
O(1)–Mn(1)–O(3)	94.17(5)	O(1)–Mn(1)–O(112)	174.50(6)	O(1)–Mn(1)–N(11)	87.87(6)
O(1)–Mn(1)–N(32)	88.27(6)	O(3)–Mn(1)–O(112)	90.60(6)	O(3)–Mn(1)–N(11)	102.02(6)
O(3)–Mn(1)–N(32)	102.87(6)	O(112)–Mn(1)–N(11)	88.45(6)	O(112)–Mn(1)–N(32)	93.35(6)
N(11)–Mn(1)–N(32)	155.02(7)	O(1)–Mn(2)–O(2)	90.97(5)	O(1)–Mn(2)–O(212)	178.90(6)
O(1)–Mn(2)–N(12)	87.07(6)	O(1)–Mn(2)–N(21)	89.51(6)	O(2)–Mn(2)–O(212)	89.19(6)
O(2)–Mn(2)–N(12)	106.01(6)	O(2)–Mn(2)–N(21)	117.60(6)	O(212)–Mn(2)–N(12)	93.92(6)
O(212)–Mn(2)–N(21)	89.46(6)	N(12)–Mn(2)–N(21)	136.30(6)	O(1)–Mn(3)–O(5)	93.65(6)
O(1)–Mn(3)–O(312)	173.12(6)	O(1)–Mn(3)–N(22)	89.61(6)	O(1)–Mn(3)–N(31)	87.84(6)
O(5)–Mn(3)–O(312)	92.98(6)	O(5)–Mn(3)–N(22)	94.27(6)	O(5)–Mn(3)–N(31)	96.77(6)
O(312)–Mn(3)–N(22)	91.76(6)	O(312)–Mn(3)–N(31)	89.53(6)	N(22)–Mn(3)–N(31)	168.80(6)
Mn(1)–O(1)–Mn(2)	112.65(6)	Mn(1)–O(1)–Mn(3)	124.28(6)	Mn(2)–O(1)–Mn(3)	122.73(7)

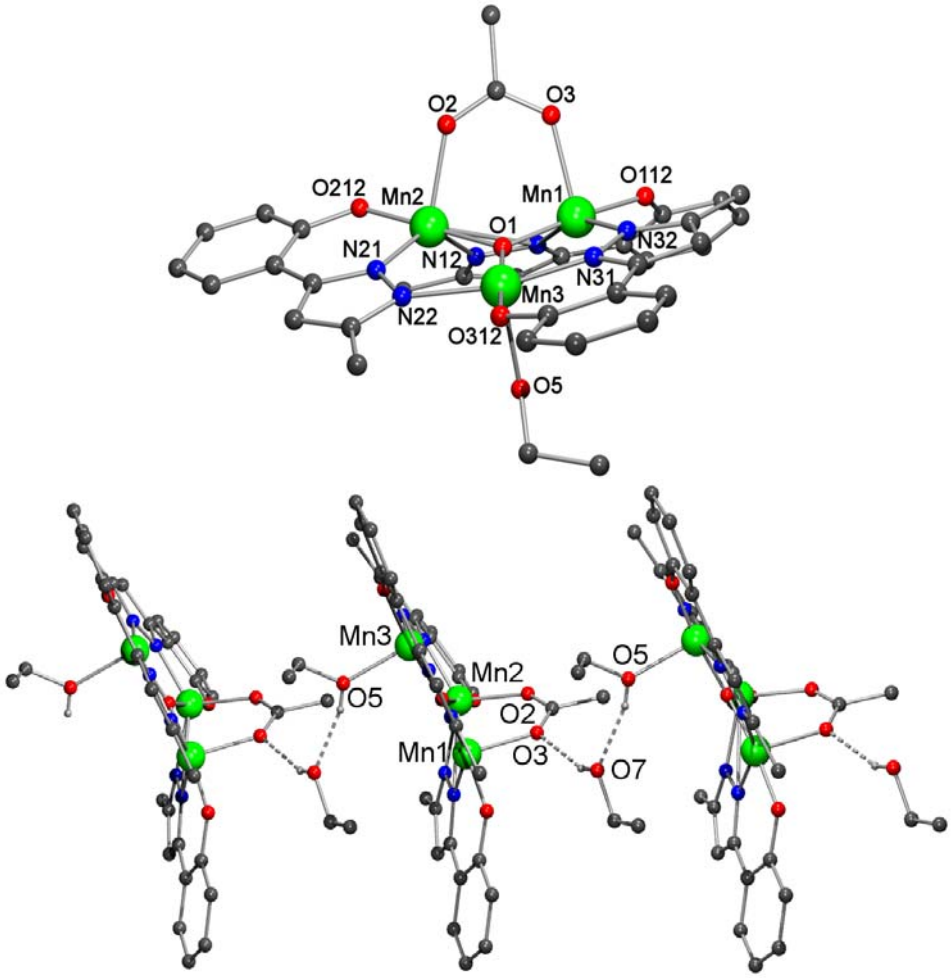

Figure 4.1. Pluton projection of the molecular structure of $[Mn_3(\mu_3\text{-}O)(phpzMe)_3(O_2CMe)(EtOH)]\cdot EtOH$(**13**) showing the detailed $Mn^{III}{}_3O$ unit (top) and the crystal packing (bottom) showing the hydrogen bonding interactions and the non-coordinated ethanol molecule. Hydrogen atoms that are not involved in hydrogen bonds are omitted for clarity. Colour code: green, manganese; blue, nitrogen; red, oxygen; grey, carbon.

Compounds **14** and **15** crystallize in the monoclinic space group $P2_1/c$ and in the triclinic space group P–1, respectively. Their molecular structures are shown in Figures 4.2 and 4.3. For both compounds, the crystallographic analyses reveal a trinuclear manganese(III) unit containing a μ_3-oxide bridge. Each edge of the Mn_3 triangle is bridged by a η^1,η^1,μ-pyrazolato ligand with the phenolic oxygen and one pyrazole nitrogen atom chelating a manganese(III) ion. Selected bond lengths and angles are listed in Table 4.3 and Table 4.4 for both compounds **14** and **15**, respectively. For compound **14**, intracluster Mn···Mn distances are 3.299 Å, 3.214 Å and 3.224 Å for Mn(1)···Mn(2), Mn(1)···Mn(3) and Mn(2)···Mn(3), respectively. For compound **15**, intracluster Mn···Mn distances are 3.350 Å, 3.209 Å and 3.250 Å for Mn(1)···Mn(2), Mn(1)···Mn(3) and Mn(2)···Mn(3), respectively. The μ_3-O^{2-} (O1) ion lies 0.029 Å above the Mn_3 plane for compound **14** and 0.001 Å for compound **15**,

respectively. In compound **14**, the Mn–O(1)–Mn angles are Mn(1)–O(1)–Mn(2) = 124.67(9)º, Mn(1)–O(1)–Mn(3) = 117.35(8)º and Mn(2)–O(1)–Mn(3) = 117.91(10)º; whereas in compound **15**, the Mn–O(1)–Mn angles are Mn(1)–O(1)–Mn(2) = 125.59(9)º, Mn(1)–O(1)–Mn(3) = 116.66(8)º and Mn(2)–O(1)–Mn(3) = 117.75(9)º. For both compounds, one manganese(III) ion is hexacoordinated and the other two manganese(III) ions are pentacoordinated. The shortest intermolecular Mn···Mn distance is 8.816 Å and 7.228 Å for compounds **14** and **15**, respectively. Therefore in the case of **15**, π–π stacking interactions (3.717 Å) are present between the pyrazole ring of one trinuclear unit and the phenol ring of the closest trinuclear unit, with a dihedral angle between the rings of 6.92º. The main difference with compound **13** is the presence of two bridging benzoate ligands in **14** and **15**, and the $^{n}Bu_4N^+$ as a counter ion, whereas in compound **13** only one bridging acetate is present. As consequence, the coordination sphere of the manganese(III) ions in **13** is completed with solvent molecules. In **13** the solvent present in the lattice is involved in hydrogen bonding that links the trinuclear units, thus forming a chain. Compounds **14** and **15** are isolated trinuclear units.

Table 4.3. Selected bonds lengths [Å] and angles [º] for $^{n}Bu_4N[Mn_3(\mu_3\text{-}O)(phpzMe)_3(O_2CPh)_2]$ (**14**).

Bond Lengths					
Mn(1)–O(1)	1.8615(18)	Mn(1)–O(58)	2.0648(16)	Mn(1)–O(112)	1.835(2)
Mn(1)–N(11)	1.9704(19)	Mn(1)–N(22)	2.0354(19)	Mn(2)–O(1)	1.8629(17)
Mn(2)–O(48)	2.0035(17)	Mn(2)–O(212)	1.8515(18)	Mn(2)–N(21)	1.953(2)
Mn(2)–N(32)	2.0740(18)	Mn(3)–O(1)	1.9006(16)	Mn(3)–O(49)	2.2987(18)
Mn(3)–O(59)	2.274(2)	Mn(3)–O(312)	1.8627(16)	Mn(3)–N(12)	2.011(2)
Mn(3)–N(31)	1.9515(19)	Mn(1)···Mn(2)	3.299	Mn(1)···Mn(3)	3.214
Mn(2)···Mn(3)	3.224				
Bond Angles					
O(1)–Mn(1)–O(58)	96.47(7)	O(1)–Mn(1)–O(112)	164.51(8)	O(1)–Mn(1)–N(11)	88.07(8)
O(1)–Mn(1)–N(22)	87.09(8)	O(58)–Mn(1)–O(112)	98.89(8)	O(58)–Mn(1)–N(11)	95.66(7)
O(58)–Mn(1)–N(22)	101.22(7)	O(112)–Mn(1)–N(11)	88.43(8)	O(112)–Mn(1)–N(22)	91.87(8)
N(11)–Mn(1)–N(22)	162.85(8)	O(1)–Mn(2)–O(48)	91.18(7)	O(1)–Mn(2)–O(212)	175.57(8)
O(1)–Mn(2)–N(21)	87.31(8)	O(1)–Mn(2)–N(32)	87.64(7)	O(48)–Mn(2)–O(212)	89.82(7)
O(48)–Mn(2)–N(21)	124.13(8)	O(48)–Mn(2)–N(32)	105.91(8)	O(212)–Mn(2)–N(21)	88.55(8)
O(212)–Mn(2)–N(32)	96.23(8)	N(21)–Mn(2)–N(32)	129.77(8)	O(1)–Mn(3)–O(49)	85.75(7)
O(1)–Mn(3)–O(59)	89.42(7)	O(1)–Mn(3)–O(312)	177.29(7)	O(1)–Mn(3)–N(12)	87.83(8)
O(1)–Mn(3)–N(31)	88.43(7)	O(49)–Mn(3)–O(59)	168.38(7)	O(49)–Mn(3)–O(312)	94.61(7)
O(49)–Mn(3)–N(12)	81.22(8)	O(49)–Mn(3)–N(31)	94.51(7)	O(59)–Mn(3)–O(312)	90.70(7)
O(59)–Mn(3)–N(12)	88.05(8)	O(59)–Mn(3)–O(31)	95.91(7)	O(312)–Mn(3)–N(12)	94.88(8)
O(312)–Mn(3)–N(31)	88.87(8)	N(12)–Mn(3)–N(31)	174.52(8)	Mn(1)–O(1)–Mn(2)	124.67(9)
Mn(1)–O(1)–Mn(3)	117.35(8)	Mn(2)–O(1)–Mn(3)	117.91(10)		

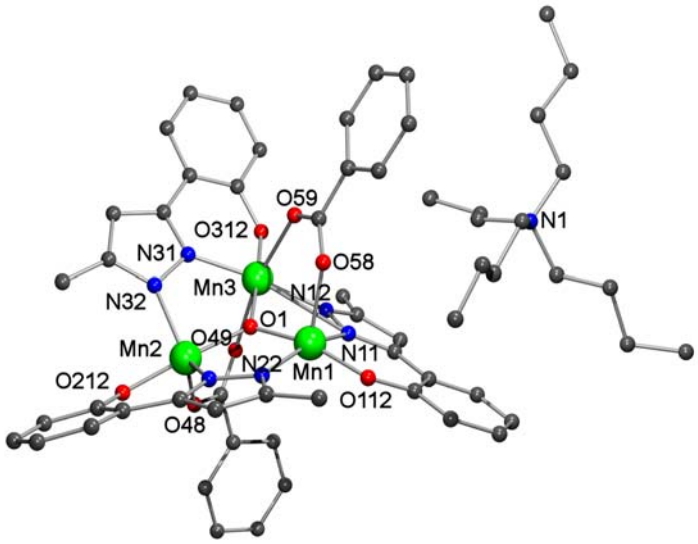

Figure 4.2. Pluton projection of the compound $^{n}Bu_4N[Mn_3(\mu_3\text{-}O)(phpzMe)_3(O_2CPh)_2]$ (**14**). Hydrogen atoms are omitted for clarity. Colour code: green, manganese; blue, nitrogen; red, oxygen; grey, carbon.

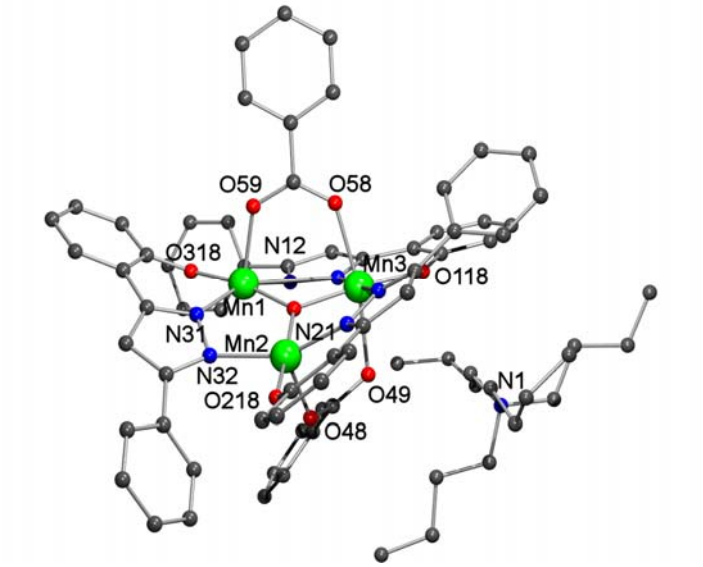

Figure 4.3. Pluton projection of the compound $^{n}Bu_4N[Mn_3(\mu_3\text{-}O)(phpzPh)_3(O_2CPh)_2]$ (**15**). Hydrogen atoms are omitted for clarity. Colour code: green, manganese; blue, nitrogen; red, oxygen; grey, carbon.

Some structural differences are observed between the trinuclear manganese(III) compounds reported here and those described previously,[12-16] all containing phenol-pyrazole ligands. The introduction of a substituent on the fifth position of the pyrazole ring, as methyl or phenyl, drives the carboxylate to bind to two manganese(III) ions from the same trinuclear unit, instead of bridging the trinuclear manganese(III) units, as was observed previously.[12,14-16] If the carboxylate ligand is small, *i.e.* acetate, these trinuclear units can form chains, because of the hydrogen bonds established between the carboxylate and the solvent molecules (*e.g.* compound **13** and $[Mn_3(\mu_3\text{-}O)(phpzMe)_3(O_2CMe)(MeOH)_3]\cdot 1.5MeOH$ (**11**)[16]). However, if the carboxylate is bulkier, such as benzoate, the trinuclear units become isolated

and no intermolecular hydrogen bonding interactions are observed. It appears that the size of the co-ligand or the solvent molecule is also an important driving force in stabilizing the type of structure as the replacement of methanol[16] by ethanol (*e.g.* compounds **14** and **15**) induces the coordination of two bridging carboxylate ligands in the same $[Mn_3(\mu_3\text{-}O)]^{7+}$ core.

Table 4.4. Selected bonds lengths [Å] and angles [º] for $^{n}Bu_4N[Mn_3(\mu_3\text{-}O)(phpzPh)_3(O_2CPh)_2]$ (**15**).

Bond Lengths					
Mn(1)–O(1)	1.8700(17)	Mn(1)–O(59)	2.0404(18)	Mn(1)–O(318)	1.8402(18)
Mn(1)–N(12)	2.051(2)	Mn(1)–N(31)	1.988(2)	Mn(2)–O(1)	1.8970(16)
Mn(2)–O(48)	2.036(2)	Mn(2)–O(218)	1.8402(18)	Mn(2)–N(21)	1.957(2)
Mn(2)–N(32)	2.053(2)	Mn(3)–O(1)	1.8999(17)	Mn(3)–O(49)	2.296(2)
Mn(3)–O(58)	2.2245(19)	Mn(3)–O(118)	1.8576(19)	Mn(3)–N(11)	1.972(2)
Mn(3)–N(22)	2.041(2)	Mn(1)···Mn(2)	3.350	Mn(1)···Mn(3)	3.209
Mn(2)···Mn(3)	3.250				
Bond Angles					
O(1)–Mn(1)–O(59)	95.25(7)	O(1)–Mn(1)–O(318)	169.72(8)	O(1)–Mn(1)–N(12)	90.00(8)
O(1)–Mn(1)–N(31)	85.93(8)	O(59)–Mn(1)–O(318)	94.47(8)	O(59)–Mn(1)–N(12)	94.81(8)
O(59)–Mn(1)–N(31)	107.59(8)	O(318)–Mn(1)–N(12)	92.55(9)	O(318)–Mn(1)–N(31)	87.93(9)
N(12)–Mn(1)–N(31)	157.50(9)	O(1)–Mn(2)–O(48)	90.01(8)	O(1)–Mn(2)–O(218)	174.03(9)
O(1)–Mn(2)–N(21)	88.46(8)	O(1)–Mn(2)–N(32)	88.18(8)	O(48)–Mn(2)–O(218)	95.91(9)
O(48)–Mn(2)–N(21)	105.74(9)	O(48)–Mn(2)–N(32)	102.85(8)	O(218)–Mn(2)–N(21)	89.20(8)
O(218)–Mn(2)–N(32)	91.24(8)	N(21)–Mn(2)–N(32)	151.21(9)	O(1)–Mn(3)–O(49)	81.99(7)
O(1)–Mn(3)–O(58)	89.54(7)	O(1)–Mn(3)–O(118)	174.95(8)	O(1)–Mn(3)–N(11)	89.96(8)
O(1)–Mn(3)–N(22)	88.65(8)	O(49)–Mn(3)–O(58)	168.40(7)	O(49)–Mn(3)–O(118)	92.97(8)
O(49)–Mn(3)–N(11)	88.65(8)	O(49)–Mn(3)–N(22)	96.10(8)	O(58)–Mn(3)–O(118)	95.41(8)
O(58)–Mn(3)–N(11)	83.51(8)	O(58)–Mn(3)–N(22)	91.60(8)	O(118)–Mn(3)–N(11)	89.60(9)
O(118)–Mn(3)–N(22)	92.22(8)	N(11)–Mn(3)–N(22)	174.92(9)	Mn(1)–O(1)–Mn(2)	125.59(9)
Mn(1)–O(1)–Mn(3)	116.66(8)	Mn(2)–O(1)–Mn(3)	117.75(9)		

Magnetic Properties. Magnetic susceptibilities were measured as a function of temperature under a 0.1 T applied field in the range 1.8–300 K. In Figures 4.4a and 4.5 the results as plots of $\chi_M T$ *vs* T are shown for, respectively, the compounds **13**–**15**. Similar as observed for other trinuclear manganese(III) compounds,[2-5,12,13,15,16,34] the $\chi_M T$ product is still increasing with temperature near room temperature and the measured $\chi_M T$ values at 300 K are therefore below the high-temperature limit of 9.00 cm^3Kmol^{-1} expected for three non-interacting manganese(III) ions. For compounds **13**, **14** and **15**, the $\chi_M T$ values measured at room temperature are 6.68 cm^3Kmol^{-1}, 6.18 cm^3Kmol^{-1}, and 6.52 cm^3Kmol^{-1}, respectively. With decreasing temperatures the $\chi_M T$ value is seen to decrease drastically in all cases. This

behaviour can be attributed to the presence of predominant intramolecular antiferromagnetic interactions (J) between the three manganese(III) ions composing the trinuclear units.[35] As a result, the magnetic energy level spectrum of the triangular units spans a wide energy range of the order of 40–70 times the magnetic exchange interaction constants (see Figure 4.6), *i.e.* amounting to a few hundreds Kelvin in thermal energy, even for J/k_B values of a few Kelvin only. As compared to the other two compounds, **13** is exceptional in that the product $\chi_M T$ passes through a minimum of 2.87 cm^3Kmol^{-1} at 30 K, increases up to about 5.26 cm^3Kmol^{-1} at 2.6 K and finally decreases again to 5.05 cm^3Kmol^{-1} at 1.8 K (Figure 4.4a). For compound **14** the $\chi_M T$ product shows a continuous gradual decrease with temperature, reaching a value of 0.67 cm^3Kmol^{-1} at 1.8 K (Figure 4.5a). For compound **15** upon cooling the $\chi_M T$ value likewise decreases continuously down to a value of 1.53 cm^3Kmol^{-1} at 15 K, and then more steeply to 0.41 cm^3Kmol^{-1} at 1.8 K (Figure 4.5b).

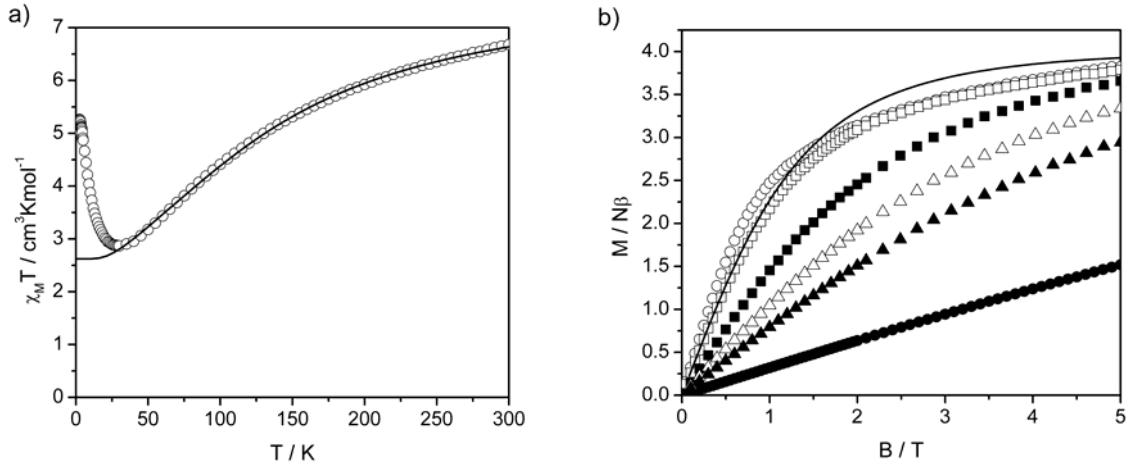

Figure 4.4. a) Plot of $\chi_M T$ *vs* T for **13** in the range 1.8 to 300 K in 0.1 T applied field with the experimental fit from 50 to 300 K (solid line). b) Field dependence of the magnetization measured at 2 (○), 4 (□), 6 (■), 8 (△), 10 (▲) and 20 (●) K. The Brillouin function (solid line) is included for one $S = 2$ and $g = 2$ at 2 K.

As will become clear from the theoretical analysis presented below, the upturn of the $\chi_M T$ product in **13** below 30 K is due to a partial ferromagnetic coupling between the manganese(III) moments within the triangular cluster, in combination with a ferromagnetic intermolecular interaction between the trinuclear units along the chains. The latter interaction will be propagated through the hydrogen bonds present between the acetate and the ethanol molecules within the 1-D chain (see Figure 4.2). For compounds **14** and **15** all intracluster interactions turn out to be antiferromagnetic.

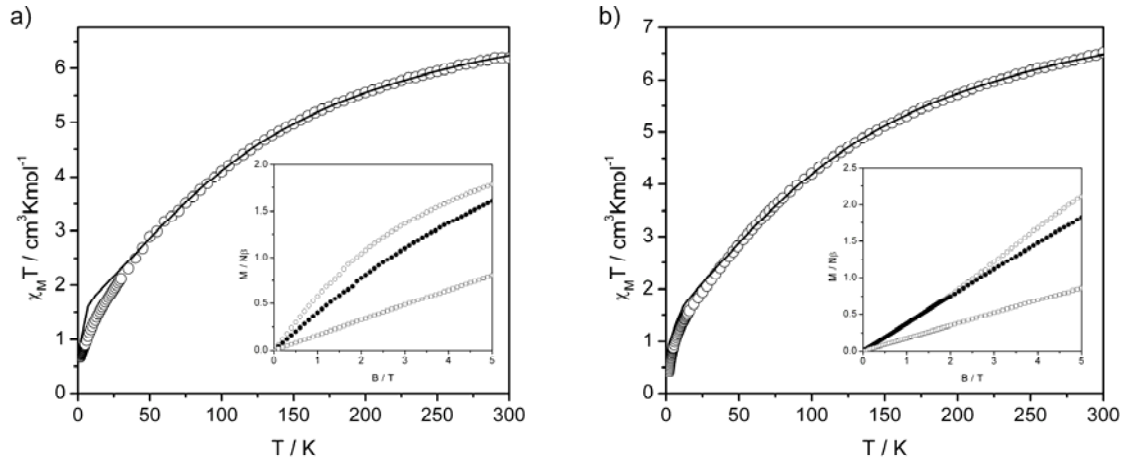

Figure 4.5. Plot of $\chi_M T$ *vs T* for **14** (a) and **15** (b) in the range 1.8 to 300 K in 0.1 T applied field with the experimental fit (solid line). Inset, field dependence of the magnetization measured at 2 (○), 4 (●) and 20 (□) K.

Field-dependent magnetization studies were carried out at low temperatures for all three materials and are shown in Figure 4.4b and as inserts in Figure 4.5. As can be noted, even at the maximum field of 5 T the values measured for the molar magnetization fall far below the saturation limit of 12 Nβ, which is appropriate for three non-interacting manganese(III) ions. This observation confirms the above-mentioned large extent in energy of the magnetic energy level spectrum for the trinuclear cluster, compared to which the Zeeman energy of the applied field is very small. Compound **13** is again exceptional in that its $M(B)$ measured at the lowest temperatures shows a fast initial increase, reaching a value of ≈ 3 Nβ at about 1 T already, not far below the 4 Nβ corresponding to one manganese(III) ion or one third of the saturated moment of the trinuclear unit. This feature again strongly suggests a partial ferromagnetic coupling within the triangle, which should result in a ground state of $S_T = 2$ for the triangular unit, as found previously also for $[Mn_3(\mu_3\text{-}O)(phpzMe)_3(MeOH)_3(O_2CMe)]\cdot 1.5MeOH$ (**11**).[16] Indeed, the experimental $M(B)$ curve for **13** at 2 K is very close to the Brillouin function for a single spin $S = 2$ calculated for that temperature, included in Figure 4.4b. At 2 K, the experimental data at lower fields (< 1 T) are slightly above this Brillouin function, indicating the presence of additional ferromagnetic intermolecular interactions, as also mentioned above in connection with the observed upturn in the magnetic susceptibility below 30 K. The behaviour of the magnetization for compounds **14** and **15**, on the other hand, indicate a low-spin magnetic ground state for the triangular units, *i.e.* all intramolecular interactions are apparently antiferromagnetic in these materials.

For a more quantitative analysis of the exchange interactions, the susceptibility data were fitted with the Hamiltonian for an isosceles triangle:

$$\hat{H} = -2[J_2(\hat{S}_1\hat{S}_2)+J_1(\hat{S}_1\hat{S}_3)+J_1(\hat{S}_2\hat{S}_3)] \qquad (1)$$

where J_1 represents the Mn(III)–Mn(III) exchange interaction parameter of the two exchange paths with similar Mn···Mn distances and Mn–O_{oxide}–Mn angles, and J_2 refers to the path characterized by the unique Mn–O_{oxide}–Mn angle (Mn(1)–O(1)–Mn(2)). Briefly, the energy levels for the isosceles triangle of spins S are given by:

$$E(S_T, S^*) = -J_1[S_T(S_T+1)-S^*(S^*+1)-S(S+1)]-J_2[S^*(S^*+1)-2S(S+1)] \qquad (2)$$

Here $S^* = S_2+S_3$ and can take the values $S^* = 2S, 2S-1, ..., 0$, whereas the total spin $S_T = (S^*+S), (S^*+S-1), ..., |S^*-S|$. In Figure 4.6, the so-obtained energy spectrum is plotted as $E(S_T, S^*)/|J_1|$ *versus* the ratio $r = J_2/J_1$. For some levels the corresponding values for the total spin S_T of the trinuclear compound have been indicated. Note that the diagram shown is for antiferromagnetic (negative) values for J_1, for ferromagnetic J_1 the diagram has to be inverted.

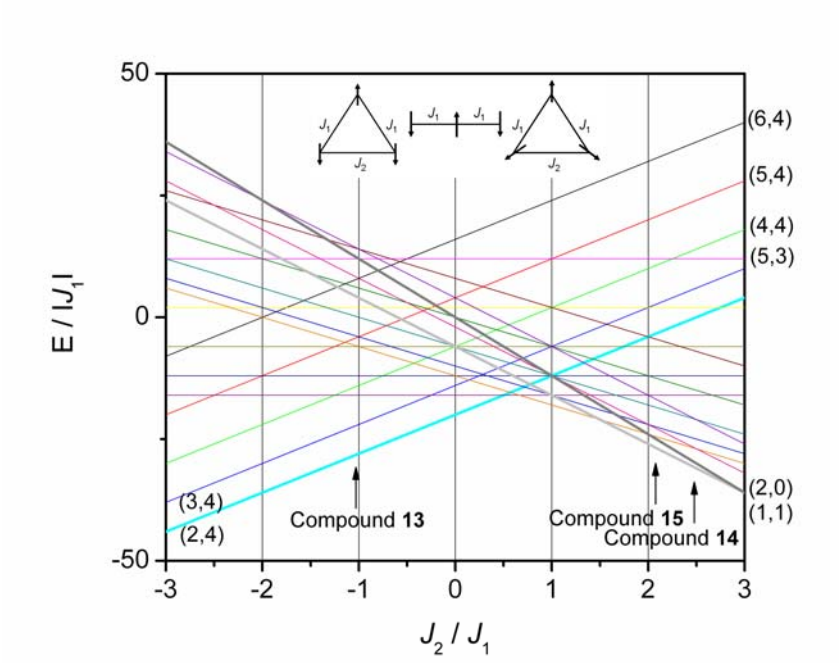

Figure 4.6. Energy levels for an isosceles triangle with $S_1 = S_2 = S_3 = 2$ calculated for $J_1 < 0$. States are labelled as (S_T,S^*).

When fitting the experimental data to these predictions one should restrict preferably to the temperature range above 50 K, to avoid the complications of intercluster interactions and zero-field manganese(III) splitting (crystal field anisotropy), which may influence the data at lower temperatures and are obviously not taken into account in the model of equation (1). On the basis of the data above 50 K, the best fitting parameters for compound **13** gave $g = 1.87 \pm$

0.03, J_1 = –(10.3 ± 0.3) cm^{-1} and J_2 = +(10.9 ± 2.4) cm^{-1}. Furthermore, the best fits of the experimental data above 50 K were g = 1.88 ± 0.02, J_1 = –(4.2 ± 0.1) cm^{-1} and J_2 = –(10.3 ± 1.2) cm^{-1} for compound **14**, and g = 1.93 ± 0.02, J_1 = –(4.8 ± 0.1) cm^{-1} and J_2 = –(10.2 ± 1.2) cm^{-1} for compound **15**. Referring to the magnetic energy level diagram calculated for the isosceles triangle as presented in Figure 4.7, one may note that the ratio $r = J_2/J_1$ equals to about −1.0 for compound **13**. This ratio corresponds indeed with an S_T = 2 ground state for the triangle, the nearest excited magnetic level being at a distance of ≈ 6 cm^{-1} in this case.

For compounds **14** and **15** r = +2.5 and +2.1 are found, respectively, corresponding to an antiferromagnetic (S_T = 1) ground state, as already anticipated above. The solid curves drawn in Figures 4.4a and 4.5 represent the predictions based on the above mentioned intramolecular magnetic exchange constants. For the purely antiferromagnetic compounds **14** and **15** the downward trend with lowering temperature of the predicted $\chi_M T$ curve is closely followed by the experiments over the whole range; the somewhat more rapid decrease of the experimental data at the lowest temperatures (≤ 15 K) can be attributed to the effects of antiferromagnetic intercluster couplings and zero-field splitting of the manganese(III) levels not considered in the Hamiltonian of equation (1). For compound **13**, on the other hand, the upturn of the experimental data below 30 K from the calculated solid curve (representing purely paramagnetic behaviour for the net spins S_T = 2 per cluster), should be ascribed to ferromagnetic intercluster couplings between the spins along the crystallographic chains. AC-susceptibility measurements were carried out on compound **13** in the range 1.8–10 K in zero DC field and at frequencies up to 997 Hz. Although no maximum in the susceptibility is yet in sight, the data do show slight frequency dependence with the appearance of an out-of-phase signal at highest frequencies. This could be interpreted either as signalling the advent of single-chain magnet behaviour or as the approach of a transition to long-range 3-D magnetic order induced by weak inter-chain interactions *e.g.* of dipolar origin. Further studies at lower temperatures (< 2 K) would be needed to clarify this behaviour.

To summarize, it has been shown that compound **13** presents both ferromagnetic and antiferromagnetic intracluster interactions, whilst only antiferromagnetic intracluster interactions are present in compounds **14** and **15**. As described in Chapter 3,[16] the occurrence of the ferromagnetic interaction in **13** can be attributed to the major distortion of the Mn–O–Mn angle of the $[Mn_3O]^{7+}$ triangle, *i.e.* Mn(1)–O(1)–Mn(2) = 112.65º. Previous theoretical and experimental studies have shown that the superexchange interaction can change from antiferromagnetic to ferromagnetic when the metal ion-ligand-metal ion angle decreases, with a the critical angle value of around 120º.[22,36] In compound **13**, the ferromagnetic interaction is stronger than observed previously[16] for

$[Mn_3(\mu_3\text{-}O)(phpzMe)_3(MeOH)_3(O_2CMe)]\cdot 1.5MeOH$ (**11**), due to the appreciably shorter Mn–O distances observed in **13** as compared to those in $[Mn_3(\mu_3\text{-}O)(phpzMe)_3(MeOH)_3(O_2CMe)]\cdot 1.5MeOH$ (**11**).[16] For compounds **14** and **15**, the deviation of the Mn–O–Mn angle from the value of 120° (corresponding to an equilateral triangle) towards lower values is less pronounced. As a consequence, all intracluster magnetic interactions are antiferromagnetic. Similar behaviour has also been reported previously in related compounds.[12,13,15,16] However, in the compounds with phenol-pyrazole ligands, the magnetic exchange interaction could be expected to also depend on the geometry of the pyrazolato bridge, as it has been shown that the dihedral angle ($\delta_{pz\text{-}bend}$) of the least-squares plane of the pyrazole ring relative to the M-N(pz)-N(pz)-M plane is also an important factor affecting the magnetic interaction.[37] Therefore Table 4.5 contains the structural and magnetic data of the $[Mn_3O]^{7+}$ compounds containing phenol-pyrazole derivatives. From this compilation it can be concluded that it is difficult to correlate the magnetic exchange parameters with this structural parameter.

As discussed above, the overall intracluster magnetic interactions are antiferromagnetic in μ_3-oxide trinuclear manganese(III) compounds with phenol-pyrazole ligands.[12-16] When the trinuclear units are linked by carboxylate bridges, ferromagnetic interactions emerge between the trinuclear units within the chain,[14-16] whilst antiferromagnetic or ferromagnetic interactions are observed when the trinuclear units are linked by end-to-end azido bridges.[13,16] In the case of the compound $[Mn_3(\mu_3\text{-}O)(Meppz)_3(EtOH)_4(O_2CMe)]$[12] in which the trinuclear units are bridged by acetate ligands, antiferromagnetic interactions are present. For the one-dimensional chains formed through hydrogen bonds established between the trinuclear units, ferromagnetic intrachain interactions are operative if the separation between the manganese(III) ions that bridge the clusters is smaller than *ca.* 7.4 Å, as it is the case for compound **13**. The intrachain interactions become antiferromagnetic for larger separation between the trinuclear units of *ca.* 8.04 Å, as observed[16] for the compound $[Mn_3(\mu_3\text{-}O)(phpzMe)_3(MeOH)_3(O_2CMe)]\cdot 1.5MeOH$ (**11**).

Table 4.5. Selected magnetic and structural data for trinuclear oxide-bridged manganese(III) compounds containing phenol-pyrazole ligands.

Compound	J_1/cm^{-1}	J_2/cm^{-1}	zJ'/cm^{-1}	g	r[b]	Mn–O–Mn[c]	$\delta_{pz\text{-}bend}$[d]	$\delta_{(MnNNMn)\text{-}(MnOMn)}$[e]	Ref
$[Mn_3(\mu_3\text{-}O)(ppz)_3(MeOH)_3(O_2CMe)]$ $[Mn_3(\mu_3\text{-}O)(phpzH)_3(MeOH)_3(O_2CMe)]$ (**10**)	–3.01	–3.01	+0.32	1.88	1.0	119.88; 119.15; 119.98	2.87; 2.50; 6.98	14.87; 2.07; 13.47	15,16
$[Mn_3(\mu_3\text{-}O)(Meppz)_3(MeOH)_4(O_2CMe)]$	–3.21	–3.21	+0.68	1.93	1.0	120.42; 119.41; 120.14	3; 3.37; 7.63	2.63; 7.91¸9.96	15
$[Mn_3(\mu_3\text{-}O)(Meppz)_3(EtOH)_4(O_2CMe)]$	–1.87	–5.61	–0.014	1.99	3.0	120.43; 118.44; 121.13	1.47; 3.60; 3.69	0.86; 6.84; 7.46	12
$[Mn_3(\mu_3\text{-}O)(Brppz)_3(MeOH)_3(N_3)]\cdot 2MeOH$	–3.87	–8.20	–0.07	2.12	2.1	119.91; 119.17; 119.35	5.89; 2.30; 4.91	6.82; 18.43; 2.35	13
$[Mn_3(\mu_3\text{-}O)(Brppz)_3(MeOH)_3(N_3)]$	–4.66	–7.35	–0.30	2.12	1.6	120.33; 118.75; 120.61	4.93; 1.47; 4.71	13.02; 14.57; 8.48	13
$[Mn_3(\mu_3\text{-}O)(Brppz)_3(MeOH)_3(O_2CMe)]$	–1.58	–5.50	–0.27	2.04	3.5	120.56; 119.18; 120.20	8.82; 2.55; 3.66	6.34; 12.50; 9.33	14
$[Mn_3(\mu_3\text{-}O)(Brppz)_3(EtOH)_3(O_2CMe)]$	–1.02	–4.39	–0.31	2.02	4.3	120.3; 119.3; 120.4	5.25; 6.37; 0.00	5.09; 2.73; 3.73	14
$[Mn_3(\mu_3\text{-}O)(Brppz)_3(EtOH)_3(O_2CMe)]$	–0.72	–3.13	–0.18	2.02	4.3	119.54; 120.15; 120.22	4.05; 2.76; 3.87	0.37; 7.71; 3.10	14
$[Mn_3(\mu_3\text{-}O)(phpzMe)_3(O_2CMe)(MeOH)_3]\cdot 1.5MeOH$ (**11**)	–7.1	+4.4	–	1.98	–0.6	120.61; 116.10; 120.85	11.97; 2.44; 24.86	12.57; 40.11; 26.02	16
$[Mn_3(\mu_3\text{-}O)(phpzH)_3(MeOH)_4(N_3)]\cdot MeOH$ (**12**)	–6.2	–3.7	–	2.01	0.6	120.79; 118.96; 120.11	4.69; 3.59; 7.12	4.51; 4.22; 1.29	16
$[Mn_3(\mu_3\text{-}O)(phpzMe)_3(O_2CMe)(EtOH)]\cdot EtOH$ (**13**)	–10.3	+10.9	–	1.87	–1.0	112.65; 122.73; 124.28	6.21; 2.89; 3.90	48.09; 7.31; 10.38	This work
$^{n}Bu_4N[Mn_3(\mu_3\text{-}O)(phpzMe)_3(O_2CPh)_2]$ (**14**)	–4.2	–10.3	–	1.88	2.5	124.67; 117.91; 117.35	2.04; 4.12; 4.57	21.41; 38.51; 37.96	This work
$^{n}Bu_4N[Mn_3(\mu_3\text{-}O)(phpzPh)_3(O_2CPh)_2]$ (**15**)	–4.8	–10.2	–	1.93	2.1	117.75; 125.58; 116.66	3.82; 3.36; 17.00	34.66; 5.13; 33.17	This work

[a] H_2phpzH = H_2ppz =5(3)-(2-hydroxyphenyl)-pyrazole, H_2Meppz = 3-(5-methyl-2-phenolate)-pyrazole, H_2Brppz = 4-bromo-2-(1-H-pyrazol-3-yl)phenol, H_2phpzMe = 3(5)-methyl-5(3)-(2-hydroxyphenyl)pyrazole. [b] $r = J_2/J_1$; [c] Mn–μ_3-O–Mn angle, Mn(1)–O–Mn(2); Mn(2)–O–Mn(3); Mn(1)–O–Mn(3) respectively; [d] dihedral angle between the pz ring plane and Mn-N(pz)-N(pz)-Mn plane; [e] dihedral angle between the Mn-N(pz)-N(pz)-Mn plane and Mn-O-Mn plane.

4.4. Conclusions

The synthesis, crystal structure and magnetic studies of three new manganese(III) compounds are reported. Compounds **13**–**15** are trinuclear μ_3-oxide-bridged manganese(III) compounds containing phenol-pyrazole ligands. Following previous results (Chapter 3),[16] the effect of the solvent or co-ligand and the type of carboxylate ligand were studied in the present work. Compound **13** forms 1-D chains due to the intermolecular hydrogen bonding between the non-coordinated ethanol molecule with the coordinated ethanol and the bridging acetate group, whereas **14** and **15** behave as isolated trinuclear manganese(III) compounds with two bridging benzoate ligands and $^{n}Bu_4N^{+}$ as a counter ion. Compounds **13**–**15** present overall intramolecular antiferromagnetic interactions between the three manganese(III) ions composing the trinuclear unit. In addition, compound **13** shows a ferromagnetic interaction between two manganese(III) ions in the trinuclear unit that can be ascribed to the most distorted structural path, resulting in a $S_T = 2$. Moreover, ferromagnetic intermolecular interactions along the chain are propagated through the hydrogen bonds.

4.5. References

1. Cannon, R. D.; White, R. P., *Prog. Inorg. Chem.,* **1988**, 36, 195-298.
2. An, J.; Chen, Z. D.; Bian, J. A.; Jin, X. L.; Wang, S. X.; Xu, G. X., *Inorg. Chim. Acta,* **1999**, 287, 82-88.
3. Baca, S. G.; Stoeckli-Evans, H.; Ambrus, C.; Malinovskii, S. T.; Malaestean, I.; Gerbeleu, N.; Decurtins, S., *Polyhedron,* **2006**, 25, 3617-3627.
4. Li, J.; Yang, S. M.; Zhang, F. X.; Tang, Z. X.; Ma, S. L.; Shi, Q. Z.; Wu, Q. J.; Huang, Z. X., *Inorg. Chim. Acta,* **1999**, 294, 109-113.
5. Vincent, J. B.; Chang, H. R.; Folting, K.; Huffman, J. C.; Christou, G.; Hendrickson, D. N., *J. Am. Chem. Soc.,* **1987**, 109, 5703-5711.
6. Wu, R. W.; Poyraz, M.; Sowrey, F. E.; Anson, C. E.; Wocadlo, S.; Powell, A. K.; Jayasooriya, U. A.; Cannon, R. D.; Nakamoto, T.; Katada, M.; Sano, H., *Inorg. Chem.,* **1998**, 37, 1913-1921.
7. Inglis, R.; Jones, L. F.; Karotsis, G.; Parsons, S.; Perlepes, S. P.; Wernsdorfer, W.; Brechin, E. K., *Chem. Commun.,* **2008**, 5924-5926.
8. Inglis, R.; Jones, L. F.; Mason, K.; Collins, A.; Moggach, S. A.; Parsons, S.; Perlepes, S. P.; Wernsdorfer, W.; Brechin, E. K., *Chem.-Eur. J.,* **2008**, 14, 9117-9121.
9. Milios, C. J.; Wood, P. A.; Parsons, S.; Foguet-Albiol, D.; Lampropoulos, C.; Christou, G.; Perlepes, S. P.; Brechin, E. K., *Inorg. Chim. Acta,* **2007**, 360, 3932-3940.
10. Xu, H.-B.; Wang, B.-W.; Pan, F.; Wang, Z.-M.; Gao, S., *Angew. Chem.-Int. Edit.,* **2007**, 46, 7388-7393.
11. Yang, C.-I.; Wernsdorfer, W.; Cheng, K.-H.; Nakano, M.; Lee, G.-H.; H.-L., T., *Inorg. Chem.,* **2008**, 47, 10184-10186.
12. Bai, Y. L.; Tao, J.; Wernsdorfer, W.; Sato, O.; Huang, R. B.; Zheng, L. S., *J. Am. Chem. Soc.,* **2006**, 128, 16428-16429.
13. Liu, C. M.; Zhang, D. Q.; Zhu, D. B., *Chem. Commun.,* **2008**, 368-370.
14. Liu, C. M.; Zhang, D. Q.; Zhu, D. B., *Inorg.Chem.,* **2009**, 48, 4980-4987.
15. Tao, J.; Zhang, Y. Z.; Bai, Y. L.; Sato, O., *Inorg. Chem.,* **2006**, 45, 4877-4879.
16. Viciano-Chumillas, M.; Tanase, S.; Mutikainen, I.; Turpeinen, U.; de Jongh, L. J.; Reedijk, J., *Inorg. Chem.,* **2008**, 47, 5919-5929.

17. Stamatatos, T. C.; Foguet-Albiol, D.; Lee, S. C.; Stoumpos, C. C.; Raptopoulou, C. P.; Terzis, A.; Wernsdorfer, W.; Hill, S. O.; Perlepes, S. P.; Christou, G., *J. Am. Chem. Soc.,* **2007**, 129, 9484-9499.
18. Stamatatos, T. C.; Foguet-Albiol, D.; Stoumpos, C. C.; Raptopoulou, C. P.; Terzis, A.; Wernsdorfer, W.; Perlepes, S. P.; Christou, G., *J. Am. Chem. Soc.,* **2005**, 127, 15380-15381.
19. Stamatatos, T. C.; Foguet-Albiol, D.; Stoumpos, C. C.; Raptopoulou, C. P.; Terzis, A.; Wernsdorfer, W.; Perlepes, S. P.; Christou, G., *Polyhedron,* **2007**, 26, 2165-2168.
20. Lampropoulos, C.; Abboud, K. A.; Stamatatos, T. C.; Christou, G., *Inorg. Chem.,* **2009**, 48, 813-815.
21. Cano, J.; Cauchy, T.; Ruiz, E.; Milios, C. J.; Stoumpos, C. C.; Stamatatos, T. C.; Perlepes, S. P.; Christou, G.; Brechin, E. K., *J. Chem. Soc.-Dalton Trans.,* **2008**, 234-240.
22. Vankalkeren, G.; Schmidt, W. W.; Block, R., *Physica B & C,* **1979**, 97, 315-337.
23. Wemple, M. W.; Tsai, H. L.; Wang, S. Y.; Claude, J. P.; Streib, W. E.; Huffman, J. C.; Hendrickson, D. N.; Christou, G., *Inorg. Chem.,* **1996**, 35, 6437-6449.
24. Addison, A. W.; Burke, P. J., *J. Heterocycl. Chem.,* **1981**, 18, 803-805.
25. Kahn, O., *Molecular Magnetism*. Wiley-VCH: New York, 1993.
26. Sheldrick, G. M. *Program for Empirical Absorption Correction*, University of Göttingen: Göttingen, Germany, 1996.
27. Beurskens, P. T.; Beurskens, G.; Strumpel, M.; Nordman, C. E., *in Patterson and Pattersons*. Glusker, J. P.; Patterson, B. K.; Rossi, M., Eds. Clarendon Press: Oxford: 1987.
28. Duisenberg, A. J. M.; Kroon-Batenburg, L. M. J.; Schreurs, A. M. M., *J. Appl. Crystallogr.,* **2003**, 220-229.
29. Duisenberg, A. J. M. Reflections on area detectors. PhD thesis, Utrecht University, Utrecht, The Netherlands 1998.
30. Beurskens, P. T.; Beurskens, G.; Bosman, W. P.; De Gelder, R.; García-Granda, S.; Gould, R. O.; Israël, R.; Smits, J. M. M.; Smykalla, C. *The DIRDIF96. A computer program system for the crystal structure determination by Patterson methods and direct methods applied to difference structure factors*, Crystallography Laboratory, University of Nijmegen: Nijmegen, The Netherlands, 1996.
31. Sheldrick, G. M. *SHELXS-97: Program for Crystal Structures Determination*, University of Göttingen: Göttingen, Germany, 1997.
32. Sheldrick, G. M. *SHELXL-97: Program for Crystal Structure Refinement*, University of Göttingen: Göttingen, Germany, 1997.
33. Spek, A. L. *PLATON, A Multipurpose Crystallographic Tool*, Utrecht University; The Netherlands, 2003.
34. Zartilas, S.; Moushi, E. E.; Nastopoulos, V.; Boudalis, A. K.; Tasiopoulos, A. J., *Inorg. Chim. Acta,* **2008**, 361, 4100-4106.
35. Martin, R. L., in *New Pathways in Inorganic Chemistry*, Ebsworth, E. A. V.; Maddock, A. G.; Sharpe, A. G., Eds. Cambridge University Press: Cambridge, 1968; pp 175-231.
36. Crawford, V. H.; Richardson, H. W.; Wasson, J. R.; Hodgson, D. J.; Hatfield, W. E., *Inorg. Chem.,* **1976**, 15, 2107-2110.
37. Tanase, S.; Koval, I. A.; Bouwman, E.; de Gelder, R.; Reedijk, J., *Inorg. Chem.,* **2005**, 44, 7860-7861.